doi:10.1093/brain/aws209 Brain 2012: 135; 2661–2675 | 2661

BRAIN
A JOURNAL OF NEUROLOGY

Lysosomal dysfunction causes neurodegeneration in mucolipidosis II 'knock-in' mice

K. Kollmann,[1,*] M. Damme,[2,*] S. Markmann,[1] W. Morelle,[3] M. Schweizer,[4] I. Hermans-Borgmeyer,[4] A. K. Röchert,[1] S. Pohl,[1] T. Lübke,[5] J.-C. Michalski,[3] R. Käkelä,[6] S. U. Walkley[7] and T. Braulke[1]

1 Department of Biochemistry, Children's Hospital, University Medical Center Hamburg-Eppendorf, 20246 Hamburg, Germany
2 Department of Biochemistry 2, Georg-August-University Göttingen, 37073 Göttingen, Germany
3 UMR CNRS/USTL 8576, Unité de Glycobiologie Structurale et Fonctionnelle, IFR 147, Bat C9, Université de Lille 1, 59655 Villeneuve d'Ascq, France
4 ZMNH, University Medical Center Hamburg-Eppendorf, 20246 Hamburg, Germany
5 Department of Biochemistry I, Faculty of Chemistry, University of Bielefeld, 33501 Bielefeld, Germany
6 Department of Biosciences, P.O. Box 65, FI-00014 University of Helsinki, Helsinki, Finland
7 Department of Neuroscience, Albert Einstein College of Medicine, Bronx, NY 10461, USA

*These authors contributed equally to this work.

Correspondence to: Thomas Braulke,
Department of Biochemistry,
Children's Hospital,
University Medical Center Hamburg-Eppendorf,
Research Campus, Martinistrasse 52,
20246 Hamburg, Germany
E-mail: braulke@uke.uni-hamburg.de

Mucolipidosis II is a neurometabolic lysosomal trafficking disorder of infancy caused by loss of mannose 6-phosphate targeting signals on lysosomal proteins, leading to lysosomal dysfunction and accumulation of non-degraded material. However, the identity of storage material and mechanisms of neurodegeneration in mucolipidosis II are unknown. We have generated 'knock-in' mice with a common mucolipidosis II patient mutation that show growth retardation, progressive brain atrophy, skeletal abnormalities, elevated lysosomal enzyme activities in serum, lysosomal storage in fibroblasts and brain and premature death, closely mimicking the mucolipidosis II disease in humans. The examination of affected mouse brains at different ages by immunohistochemistry, ultrastructural analysis, immunoblotting and mass spectrometric analyses of glycans and anionic lipids revealed that the expression and proteolytic processing of distinct lysosomal proteins such as α-L-fucosidase, β-hexosaminidase, α-mannosidase or Niemann–Pick C2 protein are more significantly impacted by the loss of mannose 6-phosphate residues than enzymes reaching lysosomes independently of this targeting mechanism. As a consequence, fucosylated N-glycans, GM2 and GM3 gangliosides, cholesterol and bis(monoacylglycero)phosphate accumulate progressively in the brain of mucolipidosis II mice. Prominent astrogliosis and the accumulation of organelles and storage material in focally swollen axons were observed in the cerebellum and were accompanied by a loss of Purkinje cells. Moreover, an increased neuronal level of the microtubule-associated protein 1 light chain 3 and the formation of p62-positive neuronal aggregates indicate an impairment of constitutive autophagy in the mucolipidosis II brain. Our findings demonstrate the essential role of mannose 6-phosphate for selected lysosomal proteins to maintain the capability for degradation of sequestered components in lysosomes and autophagolysosomes and prevent neurodegeneration. These lysosomal proteins might be a potential target for a valid therapeutic approach for mucolipidosis II disease.

Received February 27, 2012. Revised June 19, 2012. Accepted June 21, 2012

Keywords: mucolipidosis; lysosomal storage disease; trafficking of lysosomal proteins; ganglioside; impaired autophagy

Abbreviations: BMP = bis(monoacylglycero)phosphate; GlcNAc = *N*-acetylglucosamine

Introduction

Mucolipidosis type II (also known as I-cell disease) is a rare lysosomal storage disorder characterized by progressive psychomotor retardation, skeletal abnormalities, facial dysmorphism, cardiorespiratory defects and early death between 5 and 8 years of age (Leroy and Demars, 1967; Spranger and Wiedemann, 1970; Kornfeld and Sly, 2001). The disease results from defective intracellular targeting of multiple lysosomal enzymes (Kollmann *et al.*, 2010). These acid hydrolases play a critical role in cellular and tissue homeostasis and function in degradation and recycling of macromolecules, including proteins, polysaccharides, lipids, nucleic acids, glyco- and phosphoconjugates, reaching the lysosomes through the endocytic or autophagic pathway (Cox and Cachon-Gonzalez, 2012).

The efficient transport of more than 50 newly synthesized acid hydrolases to lysosomes depends on the formation of mannose 6-phosphate residues on *N*-linked oligosaccharides of these proteins that are recognized by mannose 6-phosphate-specific receptors (Hickman and Neufeld, 1972; Kaplan *et al.*, 1977; Sleat *et al.*, 2006; Braulke and Bonifacino, 2009; Lübke *et al.*, 2009). The first step in the synthesis of the mannose 6-phosphate recognition marker is catalyzed by a hexameric ($\alpha_2\beta_2\gamma_2$) *N*-acetylglucosamine (GlcNAc)-1-phosphotransferase complex encoded by the genes *GNPTAB* and *GNPTG*. *GNPTAB* encodes an enzymatically inactive precursor protein of 1256 amino acids that spans the membrane twice (Kudo *et al.*, 2005; Tiede *et al.*, 2005*a*) and is proteolytically cleaved by the site-1 protease to form catalytically active α- and β-subunits (Marschner *et al.*, 2011). *GNPTG* encodes the functionally undefined soluble γ-subunits of the phosphotransferase complex (Raas-Rothschild *et al.*, 2000).

Homozygous or compound heterozygous nonsense or frameshift mutations in *GNPTAB* leading to mucolipidosis II are characterized by the total loss of GlcNAc-1-phosphotransferase activity and of a mannose 6-phosphate recognition marker on lysosomal hydrolases, whereas missense mutations in *GNPTAB* are often associated with residual phosphotransferase activity causing a milder more slowly progressive disease, mucolipidosis III (Tiede *et al.*, 2005*b*; Kudo *et al.*, 2006; Cathey *et al.*, 2010). The subsequent missorting and hypersecretion of lysosomal enzymes is detectable in sera of patients with mucolipidosis II, and the intracellular enzyme deficiency results in lysosomal dysfunction and accumulation of non-degraded material.

A few animal models of mucolipidosis II have been described that exhibit distinct biochemical symptoms and pathological features of the human disease. Domestic short-hair cats carrying a mutation in *GNPTAB* (c.2655C > T) have been discovered, exhibiting facial dysmorphism, dysostosis multiplex, behavioural dullness and ataxia as leading symptoms and early death. Fibroblasts show excessive missorting of multiple lysosomal hydrolases, which were elevated in the serum (Bosshard *et al.*, 1996; Mazrier *et al.*, 2003). A second model of mucolipidosis II, *GNPTAB*-depleted zebrafish embryos, exhibits skeletal abnormalities, craniofacial defects and impaired motility allowed studies during early developmental stages and revealed changes in timing and expression of chondrogenic factors associated with altered chondrocyte differentiation and intracellular matrix homeostasis (Flanagan-Steet *et al.*, 2009; Petrey *et al.*, 2012). Recently, a *Gnptab* gene trap mouse model was described displaying elevated levels of serum acid hydrolases, reduced size, retinal degeneration and vacuolization in secretory epithelial cells of exocrine glands (Gelfman *et al.*, 2007; Vogel *et al.*, 2009). The mice, however, exhibited a relatively normal lifespan and failed to develop severe skeletal abnormalities.

To explore the mechanism behind neurodegenerative processes in mucolipidosis II, we generated a *Gnptab*-defective mouse by single base insertion corresponding to a mutation detected in a patient with mucolipidosis II (Tiede *et al.*, 2005*a*). These 'knock-in' mice are severely affected and show all of the clinical and biochemical symptoms and features of the mucolipidosis II disease in humans. The detailed analysis of storage material and lysosomal components in the brain led to the identification of a distinct group of lysosomal proteins such as α-L-fucosidase, β-hexosaminidase, α-mannosidase and Niemann–Pick C2 protein that require mannose 6-phosphate residues more than others to maintain lysosomal and autophagic functions and prevent neurodegeneration in mucolipidosis II.

Materials and methods

Antibodies and lectins

The following antibodies were used: anti-CD68 antibody (clone FA-11), AbD (Serotec); anti-p62 antibody (ENZO Life Sciences); glycerinaldehyde-3-phosphate dehydrogenase and beclin1 antibodies (Santa Cruz Biotechnology); anti-GM2 antibody (hydridoma clone 10-11; Progenics Pharmaceuticals); anti-GM3 antibody (clone DH2; GlycoTech); anti-β-tubulin (clone 9E10) and anti-Lamp1 (1D4B) antibody (Developmental Studies Hybridoma Bank); anti-microtubule-associated protein 1 light chain 3 antibody (LC3; clone 2G6), nanotools; anti-neuronal nuclei, anti-myelin binding protein and anti-manganese superoxide dismutase antibodies (Millipore); anti-cathepsin B antibody (Acris Antibodies); anti-glial fibrillary acidic protein (clone G-A-5), anti-calbindin (clone CB-955), anti-myc antibodies and filipin complex from *Streptomyces filipinensis* (F9765; Sigma-Aldrich). Biotinylated *Lotus tetragonolobus* and *Aleuria aurantia* lectins were purchased from Vector laboratories. Rabbit Niemann–Pick C2 protein anti-serum was a kind gift from Dr S. C. Patel (Ong *et al.*, 2004). The polyclonal antibody against cathepsin D and the myc-tagged single-chain antibody fragment against mannose 6-phosphate residues have been described previously (Claussen *et al.*, 1997; Müller-Loennies *et al.*, 2010). Secondary antibodies and streptavidin coupled to Alexa® Fluor 488 and 546 or horseradish peroxidase were purchased from Invitrogen and Jackson ImmunoResearch.

Generation of *Gnptab*$^{c.3082insC}$ mice

Targeting vector construction and 'knock-in' strategy have been designed and performed by genOway (Supplementary Fig. 1). The generation and genotyping procedure of the *Gnptab*$^{c.3082insC}$ mice are described in Supplementary Fig. 2 and in the Supplementary methods. After deletion of the *neomycin* cassette by crossing with FLPe-expressing mice (Rodriguez *et al.*, 2000), the resulting heterozygous *Gnptab*$^{c.3082insC}$ mice were inbred to yield homozygous *Gnptab*$^{c.3082insC}$. Experiments were performed with mice in a mixed C57Bl/6–129/SvJ genetic background, always using littermates as controls. Mice were housed in a pathogen-free animal facility at the University Medical Center, Hamburg-Eppendorf, and experimental procedures were performed according to the institutional guidelines.

Immunohistochemistry and ultrastructural analysis

Methods for tissue fixation and subsequent immunohistochemistry, including lectin staining and filipin labelling, were performed as described previously (Micsenyi *et al.*, 2009; Müller-Loennies *et al.*, 2010; Damme *et al.*, 2011). Ultrastructural analyses were conducted as described previously (Weinert *et al.*, 2010).

Analysis of lipids and oligosaccharides

Oligosaccharides from brain tissue were extracted as described previously (Roces *et al.*, 2004), identified by matrix-assisted laser desorption/ionization-time of flight (MALDI-TOF) mass spectrometry and gas chromatography–mass spectrometry linkage analysis (Morelle *et al.*, 2005*a, b*) and quantified by high-performance liquid chromatography (Blanz *et al.*, 2008).

Total lipids were extracted and separated into a neutral and an anionic fraction by reversed-phase C18 columns (Varian), as described previously (Jabs *et al.*, 2008). Aliquots of the neutral and anionic lipid fractions were analysed by electrospray ionization–mass spectrometry also using tandem mass spectrometry and lipid class-specific detection modes (Käkelä *et al.*, 2003; Jabs *et al.*, 2008).

Further methods

The enzymatic activity of lysosomal enzymes was assayed by estimation of 4-nitrophenol, 4-nitrocatechol, 4-methylumbelliferone or 7-amino-4-methylcoumarin liberated from the hydrolase-specific substrates. Details about the substrates, the standard assay mixture, incubation times and preparation of protein extracts are described in the Supplementary material. Real-time PCR and western blot analysis were described previously (Müller-Loennies *et al.*, 2010; Marschner *et al.*, 2011). Details about preparation of detergent-insoluble protein fractions are described in the Supplementary material.

Statistical analysis

Data were analysed by two-tailed Student *t*-test. For all graphs, data are represented as mean ± standard deviation.

Results

Generation of *Gnptab*$^{c.3082insC}$ mice and functional analysis of *Gnptab* gene inactivation

To explore the pathogenetic course and mechanisms of neurodegeneration in mucolipidosis II, we generated 'knock-in' mice in which the patient mutation *GNPTAB* c.3145insC (Tiede *et al.*, 2005*a*) was introduced into the highly homologous exon 16 of the orthologous *Gnptab* gene (Supplementary Figs 2, 3A and B). The insertion of a cytosine at position c.3082 interrupts the open reading frame of the *Gnptab* gene and changes the C-terminal conserved sequence distal to the α/β subunit precursor cleavage site, leading to a truncated GlcNAc-1-phosphotransferase protein (p.G1028RfsX16; Supplementary Fig. 3C). Western blotting of human embryonic kidney cells transfected with complementary DNA encoding wild-type and mutant α/β-subunit precursor constructs of human GlcNAc-1-phosphotransferase showed that the expression of mutant truncated α/β-subunit precursor is reduced and exhibits a slightly reduced electrophoretic mobility compared with the mature wild-type α-subunit (Supplementary Fig. 4). The data indicate that the mutant α/β-subunit precursor is not cleaved to the mature α-subunit and cannot exit the endoplasmic reticulum (Kudo and Canfield, 2006; Kollmann *et al.*, 2010).

Heterozygous crossings revealed a reduced frequency of 13% homozygous mutant mice. Mating of homozygously affected mice was successful in 10% of inter-crossings, suggesting a high infertility rate. The mutant mice were considerably smaller in size compared with wild-type siblings, and showed back deformities, additional prominent skeletal abnormalities and a flat facial profile (Fig. 1A). Growth was impaired during development, accompanied by significantly lower weight gain (Fig. 1B). Heterozygous animals did not show differences in morbidity and fertility. Compared with unaffected littermates, *Gnptab*$^{c.3082insC}$ mice displayed an increased mortality rate with a lifespan of ~64 weeks (Fig. 1C). *Gnptab*$^{c.3082insC}$ mice developed a progressive abnormality of gait and showed limb-clasping reflexes at 6 months. Early-onset photoreceptor cell degeneration in *Gnptab*$^{c.3082insC}$ mice was observed by 3–4 months of age (Supplementary Fig. 5).

The clinical diagnosis of human patients with mucolipidosis II is confirmed by (i) elevated lysosomal enzyme activities in serum; (ii) loss of GlcNAc-1-phosphotransferase activity leading to the loss of the mannose 6-phosphate targeting signal; (iii) decreased lysosomal enzyme activities in cultured fibroblasts accompanied by elevated enzyme level in the culture medium; and (iv) light microscopic presentation of prominent inclusions in patient fibroblasts (Kornfeld and Sly, 2001). In serum of *Gnptab*$^{c.3082insC}$ mice, activities of the lysosomal hydrolases β-hexosaminidase, β-galactosidase, α-mannosidase, arylsulphatase A and α-L-fucosidase were increased 2- to 11-fold compared with wild-type controls (Fig. 1D). Western blot analysis using single-chain anti-mannose 6-phosphate antibody fragments (Müller-Loennies *et al.*, 2010) revealed the total loss of mannose 6-phosphate-containing proteins in cultured *Gnptab*$^{c.3082insC}$ mouse embryonic fibroblasts.

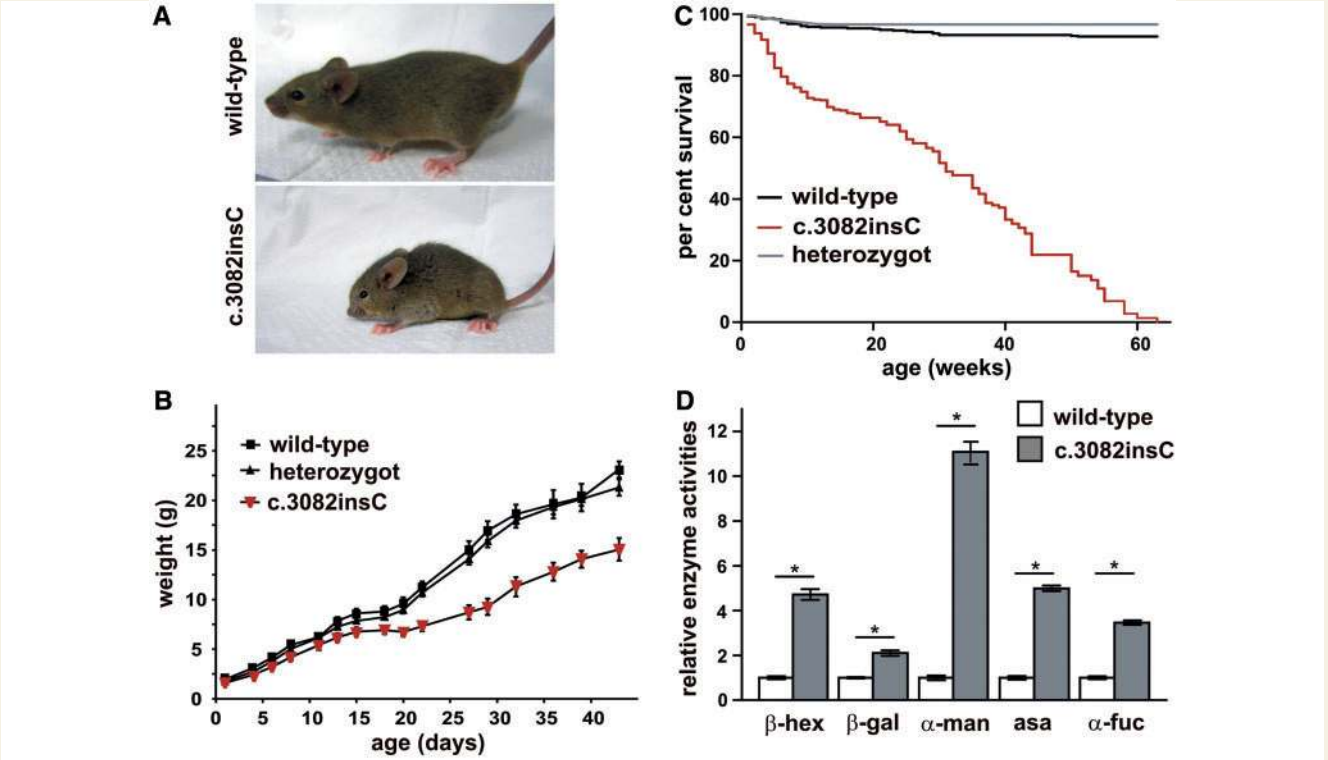

Figure 1 Phenotype of *Gnptab*$^{c.3082insC}$ mice. (**A**) One-month-old *Gnptab*$^{c.3082insC}$ mice show reduced body size and skeletal abnormalities like facial dysmorphism and curvature of the spine. (**B**) Body weight progression of *Gnptab*$^{c.3082insC}$ mice is reduced compared with wild-type and heterozygous littermates ($n = 8$, mean ± SD). (**C**) Kaplan–Meier analysis of male and female wild-type, heterozygous and homozygous *Gnptab*$^{c.3082insC}$ mice (0–20 weeks: $n = 160$, 20–40 weeks: $n = 70$, 40–60 weeks: $n = 25$). (**D**) The relative enzyme activities of the lysosomal hydrolases β-hexosaminidase (β-hex), β-galactosidase (β-gal), α-mannosidase (α-man), α-L-fucosidase (α-fuc) and arylsulphatase A (asa) were measured in sera of 6-month-old *Gnptab*$^{c.3082insC}$ mice. The specific activities of the wild-type were set to 1 (mean ± SD, $n = 3$, $^*P < 0.05$).

These fibroblasts exhibited characteristic cytoplasmic inclusion bodies (Supplementary Fig. 6A and B). The activities of several lysosomal glycosidases were found to be reduced by 50–95% in *Gnptab*$^{c.3082insC}$ fibroblasts and increased in the supernatant 3- to 18-fold. In contrast, the activities of the lysosomal proteinases cathepsin B and D were not altered in *Gnptab*$^{c.3082insC}$ compared with wild-type fibroblasts (Supplementary Fig. 6C). No alterations in the messenger RNA expression of lysosomal proteins were detected between *Gnptab*$^{c.3082insC}$ and wild-type fibroblasts (Supplementary Fig. 6C). For comparison, the transcript level of *Gnptab* was reduced in *Gnptab*$^{c.3082insC}$ mice by 75% compared with wild-type mice, whereas the expression of *Gnptg* encoding the γ-subunit of the GlcNAc-1-phosphotransferase was not changed (Supplementary Fig. 6C). In addition, the steady-state expression of cathepsin D and the lysosomal mannose 6-phosphate-containing Niemann–Pick C2 protein required for the lysosomal export of cholesterol (Deffieu and Pfeffer, 2011), was examined by western blotting. The major 40-kDa cathepsin D immunoreactive band in cell extracts represents the precursor polypeptide, which is proteolytically processed, generating a 39-kDa intermediate and a 27-kDa mature form. In *Gnptab*$^{c.3082insC}$ fibroblasts, an increased amount of the complex oligosaccharide-decorated precursor form of cathepsin D is secreted into the medium within 24 h (Supplementary Fig. 6A). Pulse-chase experiments indicate that the rate of cathepsin D synthesis is similar in *Gnptab*$^{c.3082insC}$ fibroblasts compared with wild-type fibroblasts (Supplementary Fig. 6E, lanes 1 and 3), whereas 5 h after synthesis, the amount of cathepsin D retained intracellularly was reduced owing to higher secretion into the medium (Supplementary Fig. 6E, lanes 2 and 4–6). Furthermore, the proteolytic processing of the intracellularly retained cathepsin D precursor form is altered (Supplementary Fig. 6E, lanes 2 and 4). The expression of Niemann–Pick C2 protein is strongly reduced in *Gnptab*$^{c.3082insC}$ fibroblasts in comparison with wild-type fibroblasts and missorted into the medium (Supplementary Fig. 6A). The data indicate variations in the extent of mannose 6-phosphate-dependent sorting of different lysosomal proteins and the existence of alternative protein-specific mannose 6-phosphate-independent transport routes to lysosomes. Few studies report on activities of lysosomal enzymes in human mucolipidosis II liver autopsy material showing normal or increased values (Tondeur *et al.*, 1971; Owada and Neufeld, 1982; Waheed *et al.*, 1982). In the liver homogenates of *Gnptab*$^{c.3082insC}$ mice, lysosomal enzyme activities, except cathepsin B, were significantly increased compared with wild-type liver tissue (Supplementary Fig. 7A), whereas their messenger RNA levels were unchanged (Supplementary Fig. 7B).

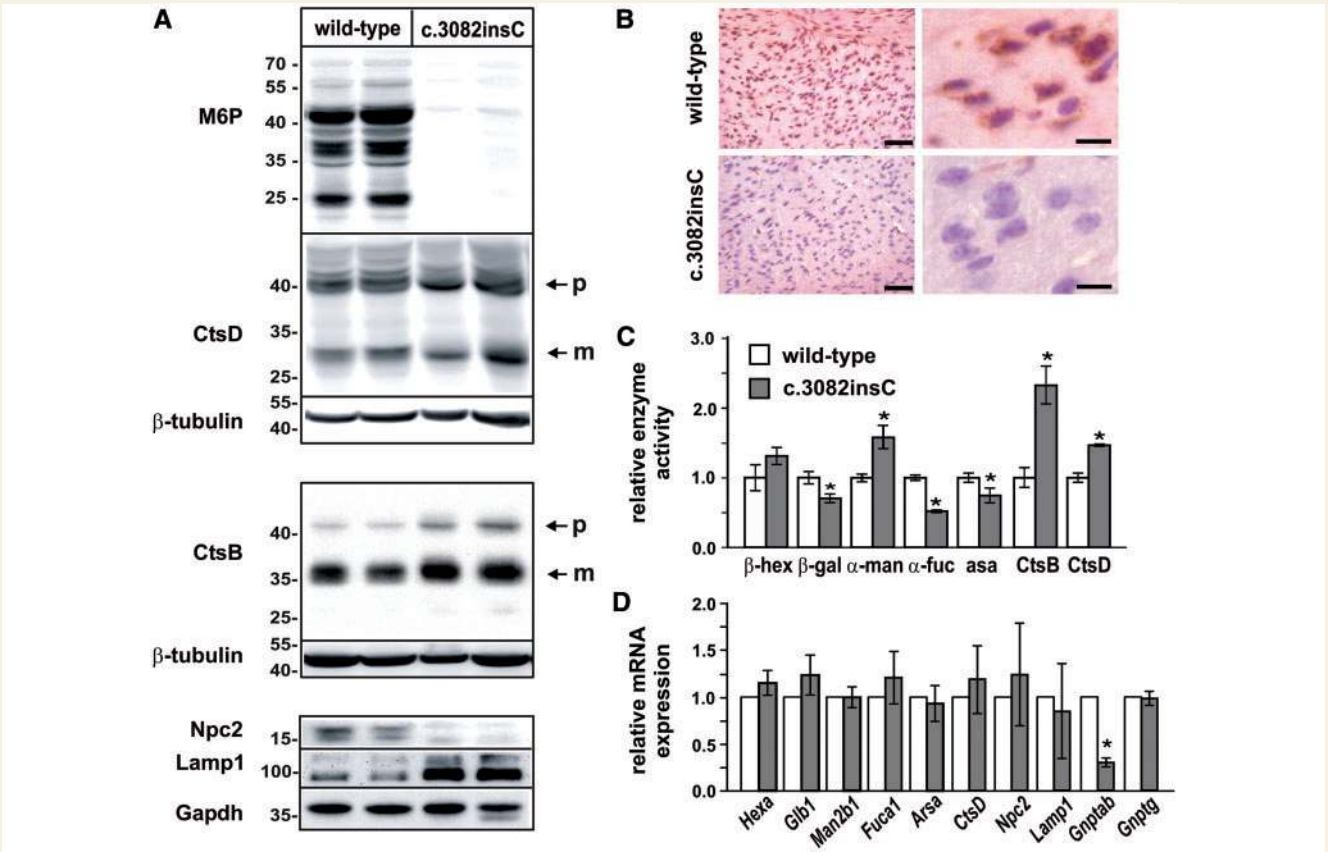

Figure 2 Expression of lysosomal enzymes in brain of *Gnptab*$^{c.3082insC}$ mice. (**A**) Brain homogenates from 4-month-old wild-type and *Gnptab*$^{c.3082insC}$ mice were analysed by western blotting using antibodies against mannose 6-phosphate residues (M6P), cathepsin D (CtsD), cathepsin B (CtsB), Npc2 and Lamp1. β-Tubulin and Gapdh were used as loading controls. p = precursor; m = mature form. (**B**) Immunodetection of M6P residues on lysosomal proteins demonstrate lack of M6P in cortical brain sections of 1-month-old *Gnptab*$^{c.3082insC}$ mice. Scale bars = 50 μm (left panel), 10 μm (right panel). (**C**) The relative enzyme activities of the lysosomal hydrolases β-hexosaminidase (β-hex), β-galactosidase (β-gal), α-mannosidase (α-man), α-L-fucosidase (α-fuc), arylsulphatase A (asa), cathepsin B (CtsB) and cathepsin D (CtsD) were measured in homogenates of perfused wild-type and *Gnptab*$^{c.3082insC}$ whole-brain tissue of 4-month-old mice. The specific activities of the wild-type were set to 1 (mean ± SD, $n = 3$, $^*P < 0.05$). (**D**) The relative messenger RNA level of the lysosomal hydrolases β-hexosaminidase (*Hexa*), β-galactosidase (*Glb1*), α-mannosidase (*Man2b1*), α-L-fucosidase (*Fuca1*) and arylsulphatase A (*Arsa*), cathepsin D (*Ctsd*), *Npc2*, *Lamp1* and the phosphotransferase subunits encoding genes *Gnptab* and *Gnptg* were determined by real-time PCR and normalized to β-actin messenger RNA expression (mean ± SD, $n = 3$, $^*P < 0.05$).

Taken together, these data clearly demonstrate that fibroblasts and liver of *Gnptab*$^{c.3082insC}$ mice exhibit the characteristic biochemical phenotype observed in patients with mucolipidosis II.

Expression of lysosomal enzymes in the brain

As shown for fibroblasts, no mannose 6-phosphate-containing proteins are detectable in the brain of *Gnptab*$^{c.3082insC}$ mice (Fig. 2A and B). Western blot analysis and densitometric evaluation revealed that the lysosomal proteases cathepsin B and cathepsin D are expressed to a similar extent (1.1- to 1.6-fold of wild-type controls) and exhibit the same proteolytic pattern in whole-brain extracts of 4-month-old wild-type and *Gnptab*$^{c.3082insC}$ mice (Fig. 2A). In contrast, Niemann–Pick C2 protein was not detectable in *Gnptab*$^{c.3082insC}$ brain tissue (Fig. 2A). Furthermore, 6.5-fold higher amounts of the lysosomal-associated membrane protein Lamp1 were found in brain extracts of *Gnptab*$^{c.3082insC}$ mice after densitometric evaluation of western blots, which is an indication of an increased number and/or size of lysosomes (Karageorgos *et al.*, 1997). When the activities of other lysosomal enzymes were measured in homogenates of perfused whole brains of 4-month-old mice, significant increased activities of α-mannosidase (1.6-fold), cathepsin D (1.5-fold) and cathepsin B (2.3-fold) were found in *Gnptab*$^{c.3082insC}$ mice, whereas mean β-hexosaminidase activity was only slightly (1.3-fold) increased (Fig. 2C). The activities of β-galactosidase, α-L-fucosidase and arylsulphatase A were significantly reduced by 25, 50 and 25%, respectively, in *Gnptab*$^{c.3082insC}$ brain (Fig. 2C). To analyse whether altered messenger RNA expression levels contribute to changes in protein

expression or enzyme activities of lysosomal proteins, quantitative real-time PCR measurements were performed on the brains of 4-month-old wild-type and *Gnptab*$^{c.3082insC}$ mice. Similar to fibroblasts or liver tissue, neither the messenger RNA expression of lysosomal enzymes nor *Gnptg* was significantly affected, whereas the transcript level of *Gnptab* was reduced in *Gnptab*$^{c.3082insC}$ mice by 75% compared with wild-type mice (Fig. 2D).

Progressive neurodegeneration in *Gnptab*$^{c.3082insC}$ mice

Macroscopic inspection of 4-month-old *Gnptab*$^{c.3082insC}$ mouse brain revealed a significant reduction in size of the cerebellum, with a reduced granular cell layer, compared with wild-type siblings (Supplementary Fig. 8A and B). Immunohistochemical staining for calbindin showed a substantial loss of Purkinje cells in 9-month-old *Gnptab*$^{c.3082insC}$ mice (Fig. 3A, *top*). Purkinje cells often exhibited severe axonal spheroid formation (Fig. 3A, arrows), a characteristic feature in several lysosomal storage diseases (Walkley *et al.*, 2010). The loss of neuronal cells and atrophy of brain tissue were progressive (Supplementary Fig. 8C) and accompanied by cerebellar demyelination with considerably thinned white matter tracts (Fig. 3B). Strong glial fibrillary acidic protein immunoreactivity was observed throughout the entire brain of *Gnptab*$^{c.3082insC}$ mice with prominent astrogliosis of the cerebellum and cerebral cortex (Fig. 3C). In the cerebellum, astrogliosis was obvious in the white matter, granular and Purkinje cell layer. Hypertrophy of the Bergmann glia was most pronounced in regions of Purkinje cell loss (Fig. 3C). Microglia activation visualized by CD68 immunoreactivity was also detected in all brain regions (Fig. 3D), with the highest intensity found in the cerebellum, cerebral cortex, hippocampus and the thalamus. Microgliosis in the cerebellum was most accented in white matter tracts and the molecular cell layer evident as early as 10 weeks of age (data not shown).

Ultrastructural analysis of the *Gnptab*$^{c.3082insC}$ mouse brain

Transmission electron microscopy was carried out to investigate the identity of lysosomal storage material accumulating in the brain of *Gnptab*$^{c.3082insC}$ mice. Abnormally increased amounts of dense bodies were found to accumulate in the majority of cortical, hippocampal and cerebellar neurons of 4-month-old *Gnptab*$^{c.3082insC}$ mice (Fig. 4A). Numerous *Gnptab*$^{c.3082insC}$ neurons exhibited swollen axons (spheroids) filled with heterogeneously appearing membrane-bound storage vacuoles (Fig. 4B–D), ranging from electron-dense to electron-lucent structures. Higher-magnification images of storage material revealed a mixture of dense and multi-lamellar bodies, electron-lucent floccular bodies, zebra bodies and fingerprint-like storage material, characteristic for accumulation of lipofuscin, glycans or glycogen and gangliosides (Fig. 4D–G). In addition, autophagosomes were found (Fig. 4G).

Accumulation of fucosylated *N*-glycans, gangliosides and bis(monoacylglycero) phosphate in the brain of *Gnptab*$^{c.3082insC}$ mice

Analysis and identification of storage material allow conclusions on lysosomal enzymes responsible for metabolic defects in lysosomal disorders. Therefore, oligosaccharide species extracted from brain of 6-month-old wild-type and *Gnptab*$^{c.3082insC}$ mice were identified by MALDI-TOF mass spectrometry. Data presented in Fig. 5A and Supplementary Fig. 9 clearly indicate that in wild-type brain, glycogen (Hex4 to Hex8) is the only detectable glycan species. In *Gnptab*$^{c.3082insC}$ brain, however, the accumulation of high mannose structures ($Hex_{2\text{-}8}HexNAc$) with variable proportions of less abundant bi- and triantennary structures was observed. In addition, fucosylated branched complex-type glycans were detected in *Gnptab*$^{c.3082insC}$ mouse brain dominated by the $Fuc_1Gal_1Man_2GlcNAc_2$ (m/z 1345) structure. Quantitative evaluation estimated ~500 pmol of $Fuc_1Gal_1Man_2GlcNAc_2$/mg brain tissue (Fig. 5B). Using *L. tetragonolobus* lectin, the accumulation of fucose-containing glycostructures was confirmed on cerebellar brain sections of 10-month-old *Gnptab*$^{c.3082insC}$ mice (Fig. 5C) showing a co-localization with the lysosomal marker protein Lamp1 in particular in the molecular layer. The data are in agreement with a currently accepted model of lysosomal *N*-glycan degradation that after release of *N*-glycans from peptide moiety by β-endo-*N*-acetylglucosaminidase, hydrolysis of terminal fucose residues by acid α-L-fucosidase initiates the stepwise cleavage of complex-type glycans (Winchester, 2005). Therefore, the loss or reduced level of α-L-fucosidase and α-mannosidase in lysosomes may contribute to the accumulation of fucosylated branched complex-type glycans and high mannose-type oligosaccharides in the brain of *Gnptab*$^{c.3082insC}$ mice.

These data are supported by *A. aurantia* lectin staining of fucose-containing glycostructures in lysosomes of cultured embryonic *Gnptab*$^{c.3082insC}$ fibroblasts. Strong reactivity of *A. aurantia* lectin was observed co-localizing with Lamp1 (Supplementary Fig. 10). In wild-type embryonic fibroblasts, a weak *A. aurantia* lectin staining in Lamp1-positive structures was detectable.

In a second approach, anionic lipids were prepared from total lipid extracts of 5- and 10-month-old mice and analysed by electrospray ionization mass spectrometry. The gangliosides were detected as precursors of m/z 290. All major ganglioside species had an 18:0 acyl and a sphingosine (d18:1) backbone. Multiple minor cationized species were present, especially for GT1. In wild-type mice, the monosialogangliosides GM2 and GM3 were barely detectable but were 1.8-fold increased in 5-month-old *Gnptab*$^{c.3082insC}$ mice (Fig. 6A and Supplementary Table 1). In addition, 1.3–1.9-fold increased concentrations of bis(monoacylglycero)phosphate (BMP) were found in *Gnptab*$^{c.3082insC}$ mice compared with wild-type mice. The most abundant BMP species was dipolyunsaturated 44:12 (22:6 n-3/22:6 n-3), constituting two-third of this lipid class (Supplementary Table 1). At the age of 10 months, the contents of GM2, GM3 and BMP increased further in *Gnptab*$^{c.3082insC}$ brain to approximately 2.3-fold higher levels than those in wild-type mice (Fig. 6B and Supplementary

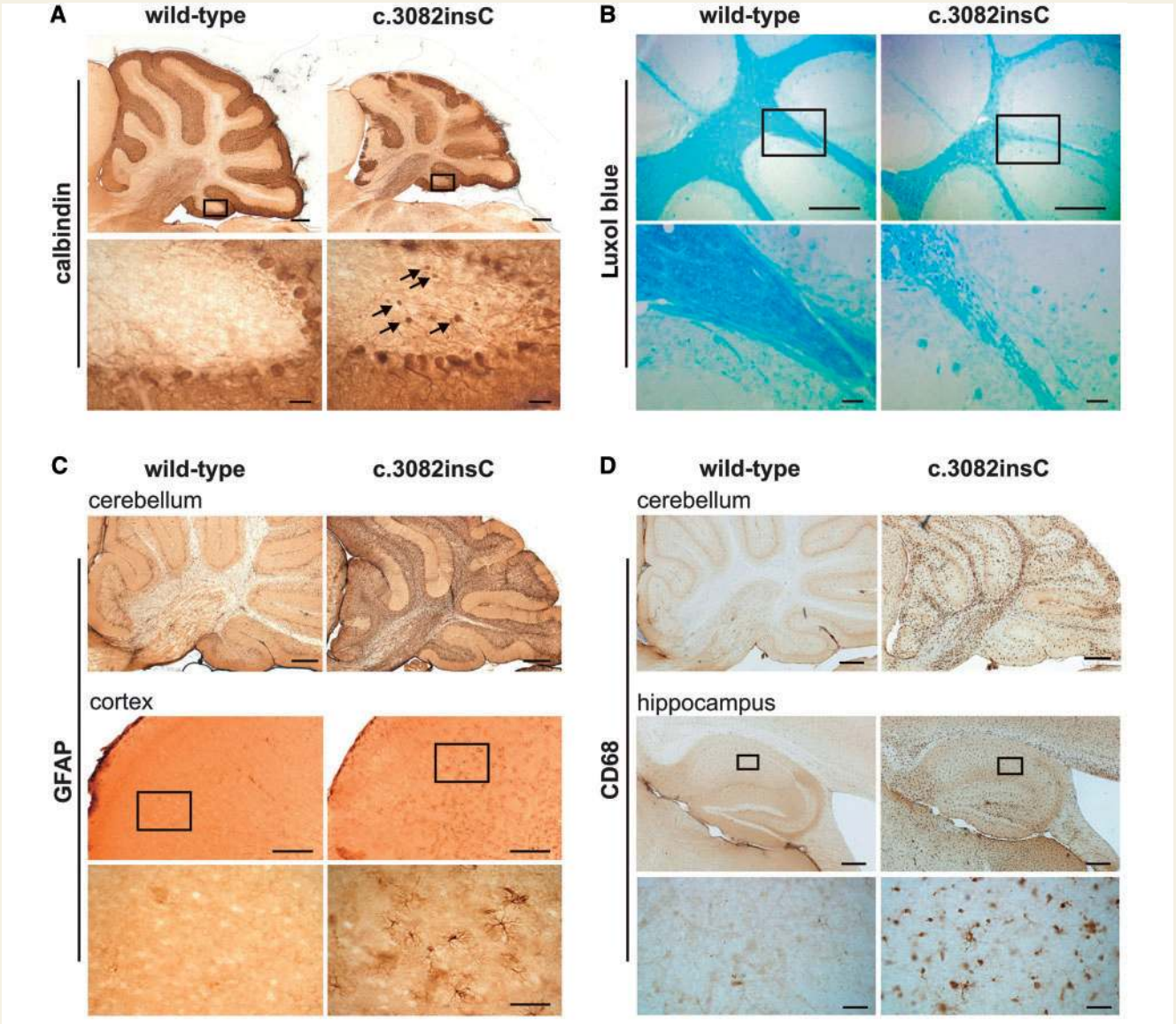

Figure 3 Pathological alterations in the brain of 9-month-old *Gnptab*$^{c.3082insC}$ mice. (**A**) Purkinje cells in cerebellar sections were stained for calbindin. Higher-magnification images of the regions marked by the black rectangles revealed axonal spheroids of Purkinje cells (arrows) in *Gnptab*$^{c.3082insC}$ mice. Scale bars: upper panel = 500 μm; insets = 50 μm. (**B**) Luxol fast blue staining of the cerebellar sections indicates decreased myelination and degeneration of the subcortical white matter in the *Gnptab*$^{c.3082insC}$ mouse. Scale bars: upper panel = 500 μm; insets = 50 μm. (**C**) Strong immunoreactivity for glial fibrillary acidic protein (GFAP) throughout the *Gnptab*$^{c.3082insC}$ brain. Insets represent higher-magnification images of the cortical region marked by the black rectangles. Scale bars: cerebellum = 500 μm; cortex = 250 μm; insets = 50 μm. (**D**) Activated microglial cells immunoreactive for CD68 are observed in the cerebellum and the hippocampus of *Gnptab*$^{c.3082insC}$ mice. Insets reveal the activated phagocytic shape of the microglial cells. Scale bars: cerebellum = 500 μm; hippocampus = 500 μm; insets = 50 μm.

Table 1). The electrospray ionization mass spectrometry analyses of the neutral glycerolipids showed no significant differences between the wild-type and *Gnptab*$^{c.3082insC}$ mice.

Immunohistochemical staining for GM2 and GM3 gangliosides confirmed their significant accumulation in vesicular structures in many neurons in the cerebral cortex as well as in hippocampal, subcortical, cerebellar and brainstem areas of *Gnptab*$^{c.3082insC}$ mice. Although neurons often appeared positive for accumulating gangliosides at 4 months of age, staining increased and was more intense and widespread by 8 months. Staining for GM2 tended to exceed that of GM3 at all ages (Fig. 6C and D). An accumulation of free cholesterol detectable by filipin histochemistry became evident coincident with ganglioside storage, with the pattern of staining appearing to most closely follow that of GM3 ganglioside. In 8-month-old *Gnptab*$^{c.3082insC}$ mice, neuronal storage of cholesterol was observed in widespread areas of the CNS. Strong filipin staining was detectable in Purkinje cells and the granular layer of the cerebellum (Fig. 6E).

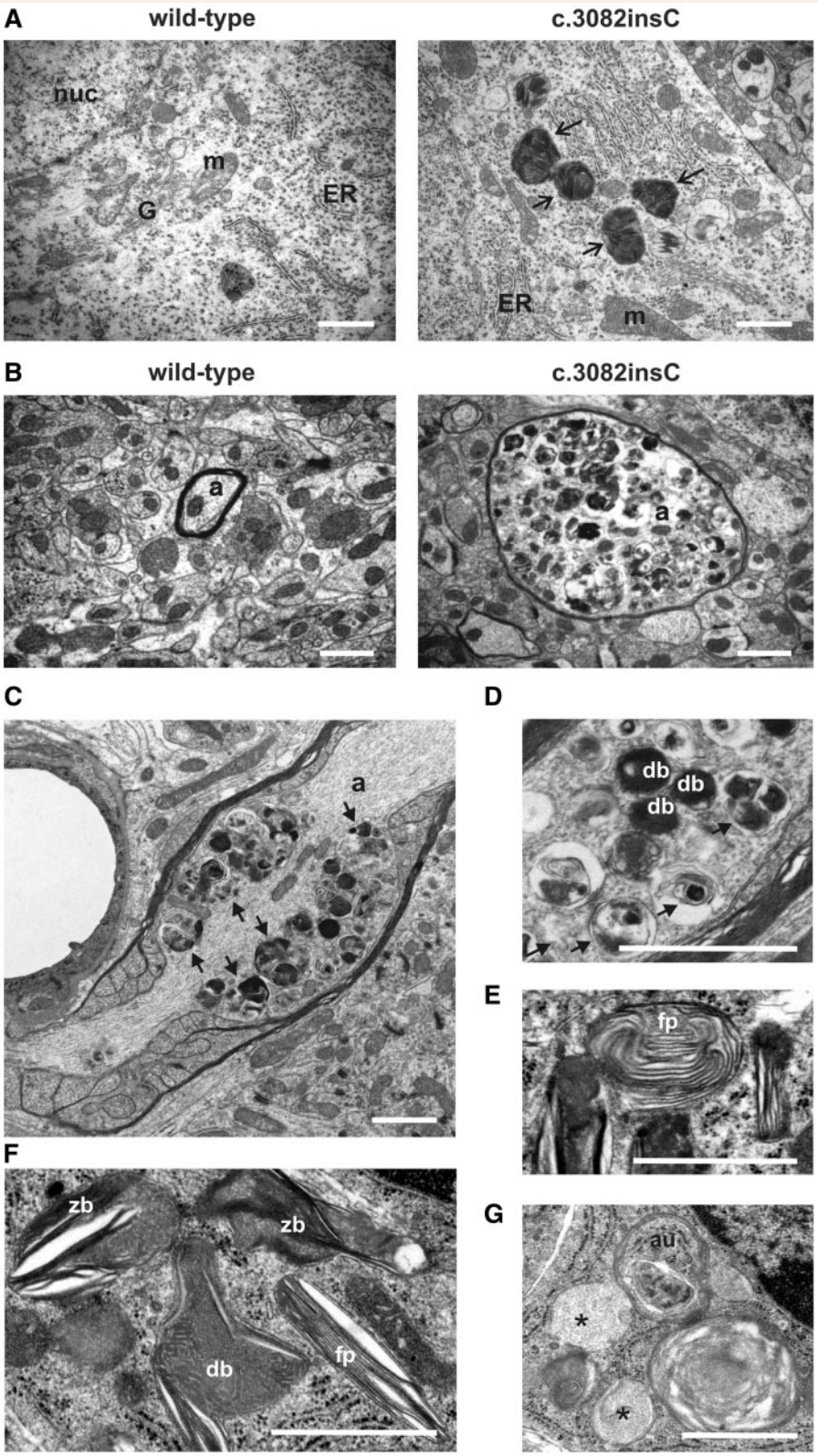

Figure 4 Ultrastructural analysis of storage material in *Gnptab*$^{c.3082insC}$ brain. (**A**) Large electron-dense inclusions (arrows) are found in the somata of hippocampal neurons from 4-month-old *Gnptab*$^{c.3082insC}$ mice. (**B**) Cross-sections of myelinated axons (a) of the cerebella from wild-type and *Gnptab*$^{c.3082insC}$ mice revealed swollen axons filled with pleomorphic granular and membranous dense bodies in 4-month-old *Gnptab*$^{c.3082insC}$ mice. (**C** and **D**) In longitudinal sections of myelinated axons (a) from 11-month-old *Gnptab*$^{c.3082insC}$ mice, the multi-vesicular accumulations (black arrows) and dense bodies (db) were clustered near the node of Ranvier. (**E** and **F**) The storage material in the cerebellar granule cells of 11-month-old *Gnptab*$^{c.3082insC}$ mice forms fingerprint bodies (fp), zebra bodies (zb) and dense bodies (db). (**G**) Vesicular structures with floccular storage material (black asterisks), and autophagosomes (au) are also found in granule cells. nuc = nucleus; m = mitochodrium; G = Golgi apparatus; ER = endoplasmatic reticulum; a = axon. Scale bars = 1 μm.

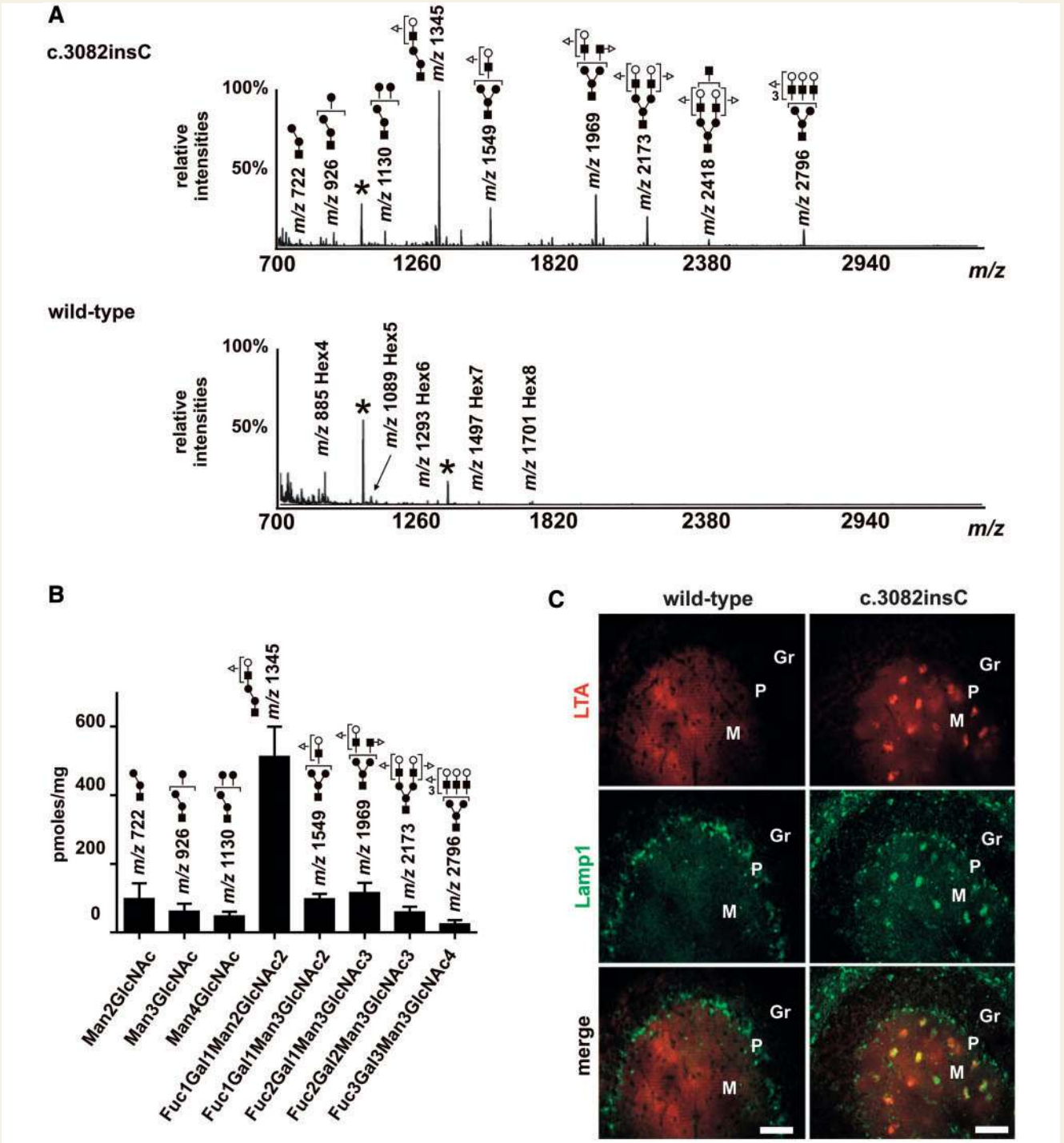

Figure 5 Analysis of the accumulating free sugar species in *Gnptab*$^{c.3082insC}$ brain. (**A**) Mass spectrometric identification of sugar species from brain extracts of 6-month-old *Gnptab*$^{c.3082insC}$ mice. Glycans were permethylated and subjected to Sep-Pak clean-up. Permethylated derivates were then analysed by MALDI-TOF mass spectrometry in the positive ion reflective mode as $[M + Na]^+$. Only the structures of the major glycans are given. In wild-type mice, glycogen (Hex4 to Hex8) is the only detectable sugar species. Black asterisks indicate contaminants from the MALDI-TOF 2,5-dihydroxybenzoic acid solution. The monosaccharides of the detected glycans are symbolically represented as follows: fucose (triangle), galactose (white circle), mannose (black circle) and *N*-acetylglucosamine (black square). (**B**) Quantification of 2-aminobenzamide-labelled oligosaccharides by high-performance liquid chromatography. (**C**) Fucosylated *N*-glycans were detected with the *L. tetragonolobus* lectin (LTA, red) by lectin fluorescence microscopy in cerebellar sections of 10-month-old *Gnptab*$^{c.3082insC}$ mice. Lysosomal membranes were stained for Lamp1 (green). M = molecular layer; P = Purkinje cell layer; Gr = granule cell layer. Scale bars = 50 μm.

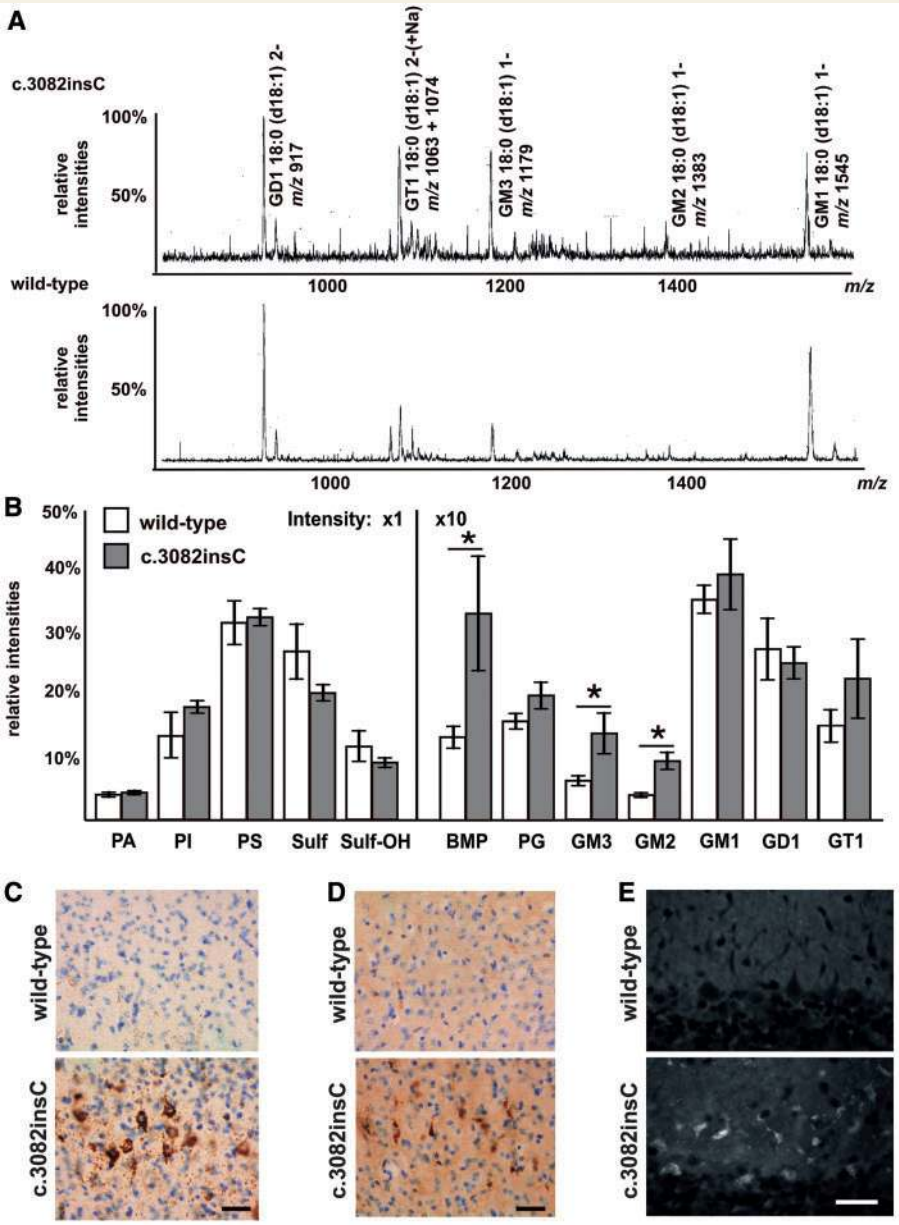

Figure 6 Analysis of the lipid profile stored in *Gnptab*$^{c.3082insC}$. (**A**) The ganglioside-containing anionic lipid fractions isolated from brain of 5-month-old *Gnptab*$^{c.3082insC}$ and wild-type mice were analysed by mass spectrometry. The gangliosides were detected as precursors of m/z 290. The gangliosides were detected either as singly charged (1-) or doubly charged (2-) ions. Multiple minor cationized species are present especially for GT1. Intensities of the spectra were normalized to the main GD1 species. (**B**) The relative changes in the totals of anionic phospholipid classes in brain extracts of 10-month-old *Gnptab*$^{c.3082insC}$ and wild-type mice. The total intensity of all anionic species detected in each sample was set to 100 (*$P < 0.05$). PA = phosphatidic acid; PI = phosphatidylinositol; PS = phosphatidylserine; Sulf = sulphatide; Sulf-OH = alpha-hydroxysulphatide; BMP = bis(monoaclylglycero)phosphate; PG = phosphatidylglycerol. (**D** and **E**) Strong GM2 immunoreactivity (**C**) and moderate GM3 immunoreactivity (**D**) were detected in the retrosplenal cortex of 8-month-old *Gnptab*$^{c.3082insC}$ mice counterstained with Nissl staining. Scale bars = 20 μm. (**E**) Cholesterol accumulation was stained by filipin in Purkinje cells and granule layer of the cerebellum of 8-month-old *Gnptab*$^{c.3082insC}$ mice. Scale bars = 20 μm.

When cultured embryonic mouse fibroblasts were analysed by double immunofluorescence microscopy, filipin staining was observed in *Gnptab*$^{c.3082insC}$ cells, which partially co-localized with Lamp1-positive lysosomal membranes (Supplementary Fig. 11). Significantly less staining for Lamp1 and cholesterol was found in fibroblasts of wild-type mice. The accumulation of fucosylated and high mannose-type oligosaccharide branches as well as sialic acid-containing GM2, GM3 gangliosides and cholesterol in the *Gnptab*$^{c.3082insC}$ brain indicates that α-L-fucosidase, α-mannosidase, β-galactosidase, sialidase and the Niemann–Pick C2 protein involved in cholesterol release from lysosomes are more affected than other lysosomal proteins by the absence of the mannose 6-phosphate recognition marker and their subsequent lysosomal localization.

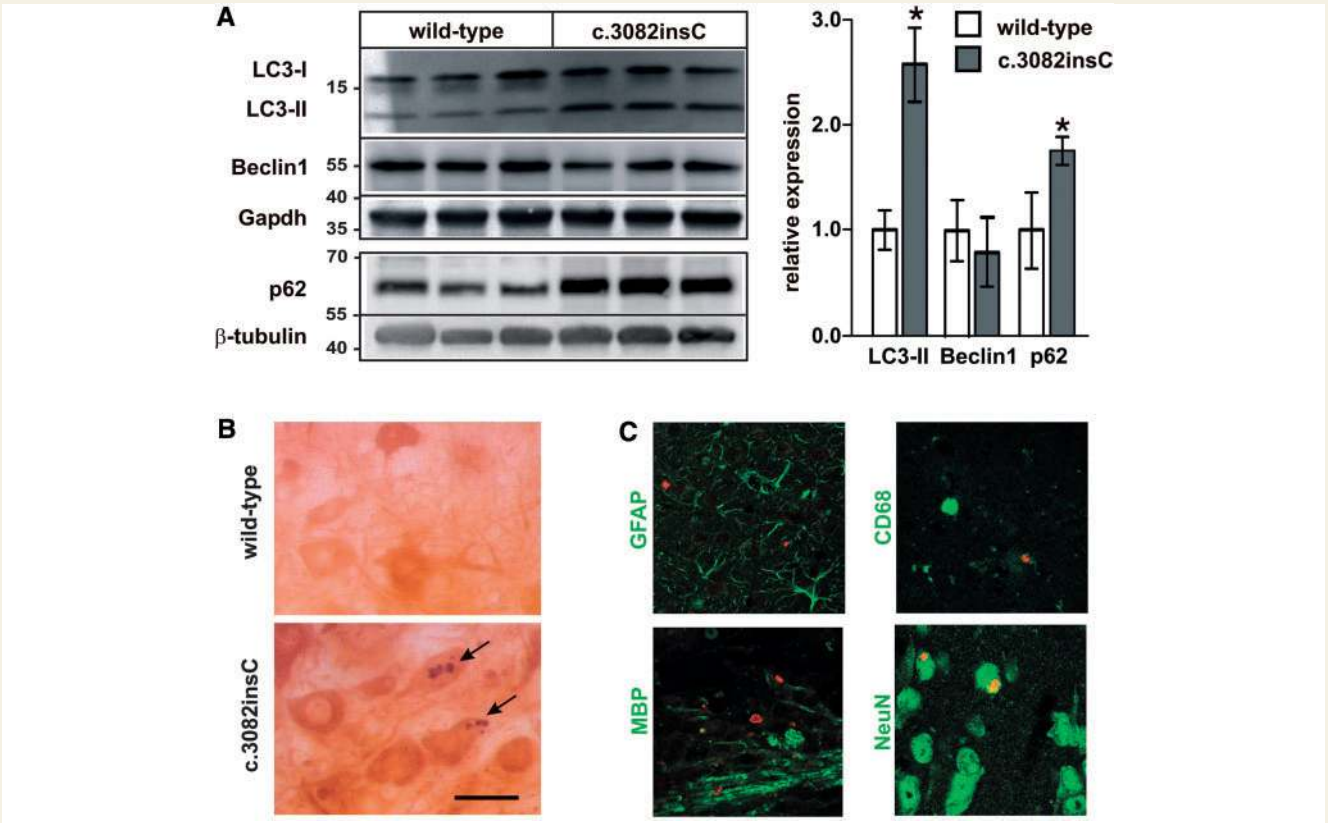

Figure 7 Accumulation of autophagosomes and p62-positive aggregates in the brain of *Gnptab*$^{c.3082insC}$ mice. (**A**) Western blot analyses and densitometric evaluation for LC3-II and beclin1 in extracts and in Triton^{TM} X-100-insoluble fractions from cerebella of 10-month-old wild-type and *Gnptab*$^{c.3082insC}$ mice (mean ± SD, $n = 3$, $^*P < 0.05$). (**B**) Immunohistochemistry for p62 showing p62 aggregates (arrows) in the soma of large neurons of the pons from 11-month-old *Gnptab*$^{c.3082insC}$ mice. Scale bars = 5 µm. (**C**) Double immunofluorescence staining reveals the co-localization of p62 (red) and the neuronal marker NeuN in *Gnptab*$^{c.3082insC}$ brain sections. No co-localization of p62 was found with marker proteins for astroglial cells (GFAP), microglial cells (CD68) and oligodendroglial cells (MBP).

Impaired autophagy and accumulation of p62 aggregates in neuronal tissue of *Gnptab*$^{c.3082insC}$ mice

To identify other cellular processes affected by dysfunctional lysosomes, the autophagy–lysosome pathway responsible for removing effete organelles and some proteins was examined in *Gnptab*$^{c.3082insC}$ brain. Disruption of autophagy is known to result in accumulation of polyubiquitinylated protein aggregates and neurodegeneration (Jansen *et al.*, 2007; Komatsu *et al.*, 2007). Western blotting showed that in brain tissue of *Gnptab*$^{c.3082insC}$ mice, the amounts of the autophagic markers lipidated LC3-II and the detergent-insoluble p62 were increased by 2.5- and 1.8-fold, respectively, compared with wild-type brain (Fig. 7A). Autophagy, however, did not appear to be activated, as evident from unchanged expression of beclin1. Immunohistochemical analysis of brain sections of 11-month-old mice revealed p62-positive aggregates throughout the brain (Fig. 7B and Supplementary Fig. 12), which were not observed in wild-type brain. Double immunofluorescence microscopy showed that p62-positive aggregates were found exclusively in anti-neuronal nuclei-immunoreactive neuronal cells of *Gnptab*$^{c.3082insC}$ mice and not in astroglial, microglial or oligodendroglial cells (Fig. 7C). These data suggest that the lysosomal dysfunction in *Gnptab*$^{c.3082insC}$ mice led to accumulation of autolysosomes in neuronal cells, which subsequently resulted in formation of p62 aggregates.

Discussion

The insertion of a single cytosine in exon 16 of *Gnptab*, corresponding to a mutation found in patients with mucolipidosis II, resulted in a clinical disease course in mice with ultrastructural, histological and biochemical findings that were highly similar to those reported in patients (Kornfeld and Sly, 2001). Birth weight and length were below normal, and affected pups revealed facial dysmorphism, severe skeletal abnormalities and premature death. In *Gnptab*$^{c.3082insC}$ mice, we observed (i) greatly increased levels of lysosomal hydrolases in serum; (ii) typical inclusion bodies in fibroblasts, as well as storage material in other tissues, including brain; and (iii) characteristic alterations in transport and activities

of lysosomal enzymes in fibroblasts and liver tissue. If the progressive neurodegeneration and gliosis observed in *Gnptab*$^{c.3082insC}$ mice also occurred in human patients with mucolipidosis II, they might be the cause for the psychomotor retardation that characterizes the human disease. These clinical features and symptoms found in human and cat mucolipidosis II and *Gnptab*$^{c.3082insC}$ mice differ from those reported for *Gnptab*$^{-/-}$ mice (Gelfman *et al.*, 2007, Vogel *et al.*, 2009). Although the liver, brain and muscle tissue appeared grossly unaffected, immunohistochemical analysis of brain sections of *Gnptab*$^{-/-}$ mice showed age-dependent lesions and widespread reactive microgliosis. In addition, the limb-clasping response observed in 4–6-month-old *Gnptab*$^{-/-}$ mice indicates neurological abnormalities (P. Vogel and S. Kornfeld, personal communication). These data suggest that at least in the *Gnptab*$^{-/-}$ brain, the pathogenic alterations represent a 'milder' course of the disease than observed in *Gnptab*$^{c.3082insC}$ mice. It is unclear whether the differences between *Gnptab*$^{-/-}$ and *Gnptab*$^{c.3082insC}$ mice are due to different mouse substrains (129S5/SvEvBrd versus 129/SvJ, respectively) used to generate the mice or secondary effects caused by the complete absence of the α/β-subunits of GlcNAc-1-phosphotransferase in the *Gnptab*$^{-/-}$ mice in comparison with low amounts of the C-terminal truncated α/β-subunit precursor localized in the endoplasmic reticulum of *Gnptab*$^{c.3082insC}$ mouse cells. It will be important to resolve this question in future studies.

In human and mouse mucolipidosis II disease, the targeting efficiency of lysosomal enzymes is variable in a cell-type- and tissue-specific manner (Owada and Neufeld, 1982, Waheed *et al.*, 1982, Boonen *et al.,* 2011). Here, we showed that the lack of mannose 6-phosphate residues in *Gnptab*$^{c.3082insC}$ mice led to a loss and missorting of the Niemann–Pick C2 protein involved in the lysosomal export of low-density lipoprotein-derived unesterified cholesterol in fibroblasts and brain. The activities of several glycosidases were strongly reduced in cultured *Gnptab*$^{c.3082insC}$ fibroblasts, whereas the activities of cathepsin B and D were comparable with wild-type cells. Furthermore, western blot and pulse-chase experiments demonstrated that distinct lysosomal enzymes, e.g. cathepsin D, can partly reach lysosomes in a mannose 6-phosphate-independent manner. Moreover, uptake of circulating lysosomal enzymes into the liver of *Gnptab*$^{c.3082insC}$ mice by various carbohydrate-specific receptors may explain the normal or increased activities of several lysosomal enzymes (Köster *et al.*, 1994). In contrast, in whole-brain extracts of *Gnptab*$^{c.3082insC}$ mice, the specific activities of e.g. β-galactosidase, α-L-fucosidase and arylsulphatase A were found to be reduced by 25–50% of wild-type brain, whereas others such as α-mannosidase, cathepsin B and cathepsin D were significantly increased. Total activity measurements as well as western blot analysis cannot distinguish between intra- and extracellular localization, which might explain the discrepancies between reduced or even increased activities of lysosomal enzymes and accumulation of non-degraded storage material. The role of alternative mannose 6-phosphate-independent transport systems with compensatory and potential selective properties for soluble proteins in lysosomal trafficking in *Gnptab*$^{c.3082insC}$ brain remains to be studied. Candidates for alternative receptor proteins are sortilin, the lysosome-integrated membrane protein 2 (Limp-2), low-density lipoprotein receptor-related protein or megalin (Hiesberger *et al.*; 1998; Lefrancois *et al.*, 2003; Nielsen *et al.*, 2007; Reczek *et al.*, 2007; Braulke and Bonifacino, 2009). The variable content of acid hydrolases and proteins in lysosomes as well as alterations in their activity due to impaired proteolytic maturation in lysosomes appear to be responsible for the clinical phenotype, which combines features of mucopolysaccharidoses and sphingolipidoses (Spranger and Wiedemann, 1970). Therefore, in mucolipidosis II, the accumulation of a variety of compounds can be expected, depending on the extent and deficiency of single or multiple proteins or enzymes, the substrate specificity of the latter and the presence of tissue-specific substrates (Ballabio and Gieselmann, 2009). This is further revealed by the ultrastructural variability of storage material in *Gnptab*$^{c.3082insC}$ mouse brain ranging from floccular and electron-opaque to electron-dense material, to membranous and zebra bodies and curvilinear and fingerprint inclusions, as have been described in the brains of patients with mucolipidosis II and cats (Martin *et al.*, 1984; Bosshard *et al.*, 1996). The appearance of these inclusions is characteristic for storage of oligosaccharides, glycosaminoglycans and glycolipids. Furthermore, the accumulation of fucosylated branched oligosaccharides in the brain and the prominent staining pattern of *L. tetragonolobus* and *A. aurantia* lectin, mainly detecting fucose in α1,3- and α1,6-linked oligosaccharides, suggest that α-L-fucosidase activity within lysosomes is significantly reduced in the brain of *Gnptab*$^{c.3082insC}$ mice. Similarly, the detection of various high mannose-type oligosaccharides in whole-brain extracts indicates decreased activity of α-mannosidase in brain lysosomes of *Gnptab*$^{c.3082insC}$ mice. Thus, the identification and compositional analysis of mucolipidosis II-associated storage material in the brain allow conclusions by which mannose 6-phosphate-containing enzymes/proteins could be thought as limiting for overall function of lysosomes.

In this study, we also found 2-fold elevated levels of GM2 and GM3 gangliosides in brain tissue of *Gnptab*$^{c.3082insC}$ mice. This might be due to reduced levels of β-hexosaminidase A and sialidase in lysosomes, respectively, or the partial loss of the mannose 6-phosphate-containing GM2 activator proteins or saposin B, which are required for the hydrolysis of GM2 and GM3 (Schulze *et al.*, 2009). Alternatively, the absence of Niemann–Pick C2 protein, which is closely associated with the storage of these gangliosides in Niemann–Pick C disease, might indirectly cause these accumulations (Walkley and Vanier, 2009). On the other hand, there are numerous other lysosomal diseases, such as mucopolysaccharidoses, neuronal ceroid lipofuscinoses and glycoproteinoses, that exhibit significant secondary accumulation of GM2 and GM3 (Walkley and Vanier, 2009), which have been implicated as possible factors causing neuron dysfunction and neurodegeneration, e.g. by the generation of toxic lyso-GM2 derivatives. In addition, the accumulation of different species of the anionic lipid BMP, required for degradation of distinct sphingolipids in brain tissue of *Gnptab*$^{c.3082insC}$ mice, support the idea that the hydrolytic functions of lysosomes are impaired. Increased levels of BMP in association with alterations in the intracellular distribution of cholesterol have also been reported in the brain of cathepsin D-deficient mice (Jabs *et al.*, 2008) and may play a critical role

in efficient sorting of lysosomal hydrolases (Kobayashi *et al.*, 1999). The accumulation of BMP in lysosomal membranes may also affect the interaction and function of lysosomal proteins as well as the degradation of distinct lipids (Gallala and Sandhoff, 2011).

The increase in LC3-II and the ubiquitin- and LC3-binding protein p62 was found to be associated with the accumulation of cytoplasmic inclusions in neuronal cells of *Gnptab*$^{c.3082insC}$ mice. An accumulation of autophagosomes containing undigested cytoplasmic material has been reported in several exocrine glands but not in the brain of *Gnptab*$^{-/-}$ mice (Boonen *et al.*, 2011). Together with the prevalence of autophagic structures, our data suggest that the constitutive autophagy responsible for the turnover of long-lived proteins, damaged organelles or removal of aggregate-prone proteins is severely impaired and might have irreversible cytotoxic effects in *Gnptab*$^{c.3082insC}$ brain. The aberrant accumulation of organelles and storage material in focally swollen axons of *Gnptab*$^{c.3082insC}$ mice, characteristic for a progressive dystrophy of axons, is similar to observations in mice with Purkinje-cell-specific loss of autophagy. The local control of axonal membrane transport and turnover by autophagy may be important in preventing axonopathy in association with neurodegeneration (Komatsu *et al.*, 2007). At present, it is not clear whether the maturation of autophagosomes into autolysosomes is inhibited in neurons of *Gnptab*$^{c.3082insC}$ mice due to the loss of hydrolytic capability of lysosomes, alterations in lysosomal membranes prohibiting the fusion between autophagosomes and lysosomes or both. Unlike the accumulation seen in neuronal cells, p62 aggregates have not been observed in glial cells of *Gnptab*$^{c.3082insC}$ mice, suggesting cell-type-specific differences in the autophagic activity.

Conclusion

The complete loss of mannose 6-phosphate residues on lysosomal enzymes resulted in a progressive neurodegeneration in *Gnptab*$^{c.3082insC}$ mice. The identification of storage material in the brain of mucolipidosis II mice demonstrated differences among lysosomal proteins in their susceptibility to the loss of mannose 6-phosphate residues. In mouse brain, the mannose 6-phosphate recognition marker is clearly more important for the targeting and/or activities of Niemann–Pick C2 protein, α-L-fucosidase, α-mannosidase or β-hexosaminidase A than for cathepsin D or cathepsin B, which can use mannose 6-phosphate-independent transport pathways to reach lysosomes in *Gnptab*$^{c.3082insC}$ brain cells. Further investigation is needed to understand these differences and to identify receptors involved. Furthermore, the efficiency of constitutive autophagic degradation appears to decline with progression of the disease, leading to neuronal accumulation of p62-associated degradation products. Thus, the generated novel mouse model of mucolipidosis II shows biochemical and clinical features of human disease and provides new insight in the role of lysosomes in degradation of brain-cell-specific substrates and into molecular mechanisms of neurodegeneration.

Acknowledgements

We thank the Microscopic Imaging Facility of the University Medical Center Hamburg-Eppendorf for using the spinning disk microscope, and Johannes Brand for technical assistance.

Funding

This work was supported by grants from the Deutsche Forschungsgemeinschaft (STO761/2-1; FOR885; GRK1459; SFB877 to K.K., S.M., A.K.R., S.P. and T.B.) and the NIH–HD045561 (S.U.W.). The mass spectrometry facility used in this study for the analysis of glycans was funded by the European Community (FEDER), the Région Nord-Pas de Calais (France) and the Université des Sciences et Technologies de Lille I.

Supplementary material

Supplementary material is available at *Brain* online.

References

Ballabio A, Gieselmann V. Lysosomal disorders: from storage to cellular damage. Biochim Biophys Acta 2009; 1793: 684–96.

Blanz J, Stroobants S, Lüllmann-Rauch R, Morelle W, Ludemann M, D'Hooge R, et al. Reversal of peripheral and central neural storage and ataxia after recombinant enzyme replacement therapy in alpha-mannosidosis mice. Hum Mol Genet 2008; 17: 3437–45.

Boonen M, van Meel E, Oorsschot V, Klumperman J, Kornfeld S. Vacuolization of mucolipidosis type II mouse exocrine gland cells represents accumulation of autolysosomes. Mol Biol Cell 2011; 22: 1135–47.

Bosshard NU, Hubler M, Arnold S, Briner J, Spycher MA, Sommerlade HJ, et al. Spontaneous mucolipidosis in a cat: an animal model of human I-cell disease. Vet Pathol 1996; 33: 1–13.

Braulke T, Bonifacino JS. Sorting of lysosomal proteins. Biochim Biophys Acta 2009; 1793: 605–14.

Cathey SS, Leroy JG, Wood T, Eaves K, Simensen RJ, Kudo M, et al. Phenotype and genotype in mucolipidosis II and III alpha/beta: a study of 61 probands. J Med Genet 2010; 47: 38–48.

Claussen M, Kübler B, Wendland M, Neifer K, Schmidt B, Zapf J, et al. Proteolysis of insulin-like growth factors (IGF) and IGF binding proteins by cathepsin D. Endocrinology 1997; 138: 3797–803.

Cox TM, Cachon-Gonzalez MB. The cellular pathology of lysosomal diseases. J Pathol 2012; 226: 241–54.

Damme M, Stroobants S, Walkley SU, Lüllmann-Rauch R, D'Hooge R, Fogh J, et al. Cerebellar alterations and gait defects as therapeutic outcome measures for enzyme replacement therapy in alpha-mannosidosis. J Neuropathol Exp Neurol 2011; 70: 83–94.

Deffieu MS, Pfeffer SR. Niemann-Pick type C 1 function requires lumenal domain residues that mediate cholesterol-dependent NPC2 binding. Proc Natl Acad Sci USA 2011; 108: 18932–6.

Flanagan-Steet H, Sias C, Steet R. Altered chondrocyte differentiation and extracellular matrix homeostasis in a zebrafish model for mucolipidosis II. Am J Pathol 2009; 175: 2063–75.

Gallala HD, Sandhoff K. Biological function of the cellular lipid BMP-BMP as a key activator for cholesterol sorting and membrane digestion. Neurochem Res 2011; 36: 1594–600.

Gelfman CM, Vogel P, Issa TM, Turner CA, Lee WS, Kornfeld S, et al. Mice lacking alpha/beta subunits of GlcNAc-1-phosphotransferase

exhibit growth retardation, retinal degeneration, and secretory cell lesions. Invest Ophthalmol Vis Sci 2007; 48: 5221–8.

Hickman S, Neufeld EF. A hypothesis for I-cell disease: defective hydrolases that do not enter lysosomes. Biochem Biophys Res Commun 1972; 49: 992–9.

Hiesberger T, Huttler S, Rohlmann A, Schneider W, Sandhoff K, Herz J. Cellular uptake of saposin (SAP) precursor and lysosomal delivery by the low density lipoprotein receptor-related protein (LRP). EMBO J. 1998; 17: 4617–25.

Jabs S, Quitsch A, Käkelä R, Koch B, Tyynelä J, Brade H, et al. Accumulation of bis(monoacylglycero)phosphate and gangliosides in mouse models of neuronal ceroid lipofuscinosis. J Neurochem 2008; 106: 1415–25.

Jansen P, Giehl K, Nyengaard JR, Teng K, Lioubinski O, Sjoegaard SS, et al. Roles for the pro-neurotrophin receptor sortilin in neuronal development, aging and brain injury. Nat Neurosci 2007; 10: 1449–57.

Käkelä R, Somerharju P, Tyynelä J. Analysis of phospholipid molecular species in brains from patients with infantile and juvenile neuronal-ceroid lipofuscinosis using liquid chromatography-electrospray ionization mass spectrometry. J Neurochem 2003; 84: 1051–65.

Kaplan A, Fischer D, Achord D, Sly W. Phosphohexosyl recognition is a general characteristic of pinocytosis of lysosomal glycosidases by human fibroblasts. J Clin Invest 1977; 60: 1088–93.

Karageorgos LE, Isaac EL, Brooks DA, Ravenscroft EM, Davey R, Hopwood JJ, et al. Lysosomal biogenesis in lysosomal storage disorders. Exp Cell Res 1997; 234: 85–97.

Kobayashi T, Beuchat MH, Lindsay M, Frias S, Palmiter RD, Sakuraba H, et al. Late endosomal membranes rich in lysobisphosphatidic acid regulate cholesterol transport. Nat Cell Biol. 1999; 1: 113–18.

Kollmann K, Pohl S, Marschner K, Encarnacao M, Sakwa I, Tiede S, et al. Mannose phosphorylation in health and disease. Eur J Cell Biol 2010; 89: 117–23.

Komatsu M, Wang QJ, Holstein GR, Friedrich VL Jr, Iwata J, Kominami E, et al. Essential role for autophagy protein Atg7 in the maintenance of axonal homeostasis and the prevention of axonal degeneration. Proc Natl Acad Sci. USA 2007; 104: 14489–94.

Köster A, von Figura K, Pohlmann R. Mistargeting of lysosomal enzymes in Mr 46000 mannose 6-phosphate receptor-deficient mice is compensated by carbohydrate-specific endocytotic receptors. Eur J Biochem 1994; 224: 685–9.

Kornfeld S, Sly WS. I-cell disease and pseudo-Hurler polydystrophy: disorders of lysosomal enzyme phosphorylation and localization. In: Scriver CR, Beaudet AL, Sly WS, Valle D, Childs B, Kinzler KW, Vogelstein B, editors. The metabolic and molecular bases of inherited disease. New York: McGraw-Hill Inc.; 2001. p. 3421–52.

Kudo M, Bao M, D'Souza A, Ying F, Pan H, Roe BA, et al. The alpha- and beta-subunits of the human UDP-N-acetylglucosamine:lysosomal enzyme N-acetylglucosamine-1-phosphotransferase [corrected] are encoded by a single cDNA. J Biol Chem 2005; 280: 36141–9.

Kudo M, Brem MS, Canfield WM. Mucolipidosis II (I-cell disease) and mucolipidosis IIIA (classical pseudo-Hurler polydystrophy) are caused by mutations in the GlcNAc-phosphotransferase α/β-subunits precursor gene. Am J Hum Genet 2006; 78: 451–63.

Kudo M, Canfield WM. Structural requirements for efficient processing and activation of recombinant human UDP-N-acetylglucosamine: lysosomal-enzyme-N-acetylglucosamine-1-phosphotransferase. J Biol Chem 2006; 281: 11761–8.

Lefrancois S, Zeng J, Hassan AJ, Canuel M, Morales CR. The lysosomal trafficking of sphingolipid activator proteins (SAPs) is mediated by sortilin. EMBO J 2003; 22: 6430–7.

Leroy JG, Demars RI. Mutant enzymatic and cytological phenotypes in cultured human fibroblasts. Science 1967; 157: 804–6.

Lübke T, Lobel P, Sleat DE. Proteomics of the lysosome. Biochim Biophys Acta 2009; 1793: 625–35.

Marschner K, Kollmann K, Schweizer M, Braulke T, Pohl S. A key enzyme in the biogenesis of lysosomes is a protease that regulates cholesterol metabolism. Science 2011; 333: 87–90.

Martin JJ, Leroy JG, van Eygen M, Ceuterick C. I-cell disease. A further report on its pathology. Acta Neuropathol 1984; 64: 234–42.

Mazrier H, Van Hoeven M, Wang P, Knox VW, Aguirre GD, Holt E, et al. Inheritance, biochemical abnormalities, and clinical features of feline mucolipidosis II: the first animal model of human I-cell disease. J Hered 2003; 94: 363–73.

Micsenyi MC, Dobrenis K, Stephney G, Pickel J, Vanier MT, Slaugenhaupt SA, et al. Neuropathology of the Mcoln1(-/-) knockout mouse model of mucolipidosis type IV. J Neuropathol Exp Neurol 2009; 68: 125–35.

Morelle W, Jimenez JC, Cieniewski-Bernard C, Dei-Cas E, Michalski JC. Characterization of the N-linked glycans of Giardia intestinalis. Glycobiology 2005a; 15: 549–59.

Morelle W, Page A, Michalski JC. Electrospray ionization ion trap mass spectrometry for structural characterization of oligosaccharides derivatized with 2-aminobenzamide. Rapid Commun Mass Spectrom 2005b; 19: 1145–58.

Müller-Loennies S, Galliciotti G, Kollmann K, Glatzel M, Braulke T. A novel single-chain antibody fragment for detection of mannose 6-phosphate-containing proteins: application in mucolipidosis type II patients and mice. Am J Pathol 2010; 177: 240–7.

Nielsen R, Courtoy PJ, Jacobsen C, Dom G, Lima WR, Jadot M, et al. Endocytosis provides a major alternative pathway for lysosomal biogenesis in kidney proximal tubular cells. Proc Natl Acad Sci USA 2007; 104: 5407–12.

Ong WY, Sundaram RK, Huang E, Ghoshal S, Kumar U, Pentchev PG, et al. Neuronal localization and association of Niemann Pick C2 protein (HE1/NPC2) with the postsynaptic density. Neuroscience 2004; 128: 561–70.

Owada M, Neufeld EF. Is there a mechanism for introducing acid hydrolases into liver lysosomes that is independent of mannose 6-phosphate recognition? Evidence from I-cell disease. Biochem Biophys Res Commun 1982; 105: 814–20.

Petrey AC, Flanagan-Steet H, Johnson S, Fan X, De la Rosa M, Haskins ME, et al. Excessive activity of cathepsin K is associated with cartilage defects in a zebrafish model of mucolipidosis II. Dis Model Mech 2012; 5: 177–90.

Raas-Rothschild A, Cormier-Daire V, Bao M, Genin E, Salomon R, Brewer K, et al. Molecular basis of variant pseudo-hurler polydystrophy (mucolipidosis IIIC). J Clin Invest 2000; 105: 673–81.

Reczek D, Schwake M, Schröder J, Hughes H, Blanz J, Jin X, et al. LIMP-2 is a receptor for lysosomal mannose-6-phosphate-independent targeting of beta-glucocerebrosidase. Cell 2007; 131: 770–83.

Roces DP, Lüllmann-Rauch R, Peng J, Balducci C, Andersson C, Tollersrud O, et al. Efficacy of enzyme replacement therapy in alpha-mannosidosis mice: a preclinical animal study. Hum Mol Genet 2004; 13: 1979–88.

Rodriguez CI, Buchholz F, Galloway J, Sequerra R, Kasper J, Ayala R, et al. High-efficiency deleter mice show that FLPe is an alternative to Cre-loxP. Nat Genet 2000; 25: 139–40.

Schulze H, Kolter T, Sandhoff K. Principles of lysosomal membrane degradation: cellular topology and biochemistry of lysosomal lipid degradation. Biochim Biophys Acta 2009; 1793: 674–83.

Sleat DE, Zheng H, Qian M, Lobel P. Identification of sites of mannose 6-phosphorylation on lysosomal proteins. Mol Cell Proteomics 2006; 5: 686–701.

Spranger JW, Wiedemann HR. The genetic mucolipidoses. Diagnosis and differential diagnosis. Humangenetik 1970; 9: 113–39.

Tiede S, Storch S, Lübke T, Henrissat B, Bargal R, Raas-Rothschild A, et al. Mucolipidosis II is caused by mutations in GNPTA encoding the alpha/beta GlcNAc-1-phosphotransferase. Nat Med 2005a; 11: 1109–12.

Tiede S, Muschol N, Reutter G, Cantz M, Ullrich K, Braulke T. Missense mutations in N-acetylglucosamine-1-phosphotransferase alpha/beta subunit gene in a patient with mucolipidosis III and a mild clinical phenotype. Am J Med Genet A 2005b; 137A: 235–40.

Tondeur M, Vamos-Hurwitz E, Mockel-Pohl S, Dereume JP, Cremer N, Loeb H. Clinical, biochemical, and ultrastructural studies in a case of chondrodystrophy presenting the I-cell phenotype in tissue culture. J Pediatr 1971; 79: 366–78.

Vogel P, Payne BJ, Read R, Lee WS, Gelfman CM, Kornfeld S. Comparative pathology of murine mucolipidosis types II and IIIC. Vet Pathol. 2009; 46: 313–24.

Waheed A, Pohlmann R, Hasilik A, von Figura K, van Elsen A, Leroy JG. Deficiency of UDP-N-acetylglucosamine: lysosomal enzyme N-acetylglucosamine-1-phosphotransferase in organs of I-cell patients. Biochem Biophys Res Commun 1982; 105: 1052–8.

Walkley SU, Sikora J, Micsenyi M, Davidson C, Dobrenis K. Lysosomal compromise and brain dysfunction: examining the role of neuroaxonal dystrophy. Biochem Soc Trans 2010; 38: 1436–41.

Walkley SU, Vanier MT. Secondary lipid accumulation in lysosomal disease. Biochim Biophys Acta 2009; 1793: 726–36.

Weinert S, Jabs S, Supanchart C, Schweizer M, Gimber N, Richter M, et al. Lysosomal pathology and osteopetrosis upon loss of H^+-driven lysosomal Cl- accumulation. Science 2010; 328: 1401–3.

Winchester B. Lysosomal metabolism of glycoproteins. Glycobiology 2005; 15: 1R–15R.